Inhibition of the MET Kinase Activity and Cell Growth in MET-Addicted Cancer Cells by Bi-Paratopic Linking

Fabio Andres [1], Luisa Iamele [2], Timo Meyer [3], Jakob C. Stüber [1], Florian Kast [1], Ermanno Gherardi [2], Hartmut H. Niemann [3] and Andreas Plückthun [1]

*1 - **Department of Biochemistry,** University of Zurich, Winterthurerstrasse 190, 8057 Zurich, Switzerland*
*2 - **Department of Molecular Medicine,** University of Pavia, Italy*
*3 - **Department of Chemistry,** Bielefeld University, Germany*

***Correspondence to Andreas Plückthun:** Department of Biochemistry, University of Zurich, Winterthurerstrasse 190, 8057 Zurich, Switzerland. plueckthun@bioc.uzh.ch*
https://doi.org/10.1016/j.jmb.2019.03.024
Edited by S. Koide

Abstract

MET, the product of the *c-MET* proto-oncogene, and its ligand hepatocyte growth factor/scatter factor (HGF/SF) control survival, proliferation and migration during development and tissue regeneration. HGF/SF-MET signaling is equally crucial for growth and metastasis of a variety of human tumors, but resistance to small-molecule inhibitors of MET kinase develops rapidly and therapeutic antibody targeting remains challenging. We made use of the designed ankyrin repeat protein (DARPin) technology to develop an alternative approach for inhibiting MET. We generated a collection of MET-binding DARPins covering epitopes in the extracellular MET domains and created comprehensive sets of bi-paratopic fusion proteins. This new class of molecules efficiently inhibited MET kinase activity and downstream signaling, caused receptor downregulation and strongly inhibited the proliferation of MET-dependent gastric carcinoma cells carrying *MET* locus amplifications. MET-specific bi-paratopic DARPins may represent a novel and potent strategy for therapeutic targeting of MET and other receptors, and this study has elucidated their mode of action.

Introduction

MET, the product of the *c-MET* proto-oncogene, is a receptor tyrosine kinase (RTK) initially discovered as TPR-MET, an oncogenic fusion protein containing the kinase domain of MET fused to a dimerization domain encoded by a translocated promotor region [1]. The physiological MET ligand is a protein known as hepatocyte growth factor/scatter factor (HGF/SF) [2]. Similar to other RTKs, MET is activated by ligand binding to the extracellular domain (ECD), which facilitates receptor dimerization, trans-phosphorylation of the kinase domains and downstream signaling. The HGF/SF-MET system regulates a set of cellular responses that initiate a coordinated biological program of cell growth and migration, leading to tissue and organ morphogenesis during development (reviewed in Ref. [3]). HGF/SF-MET signaling is essential in embryogenesis for the development of the placenta, liver, kidney and specific groups of muscle and motor neurons [3] and in post-natal life for regeneration of the liver [4] and skin [5].

The role of HGF/SF and MET in progression and metastasis of a variety of human tumors is equally compelling [6]. Receptor-activating mutations occur in hereditary kidney cancer [7], papillary renal cancer [8], hepatocellular carcinoma [9], gastric cancer [10] and their metastases [11]. Osteosarcomas, rhabdomyosarcomas and glioblastoma [12] secrete HGF/SF and express MET, thus activating autocrine MET signaling. On the other hand, overexpression of MET, as a result of transcriptional upregulation, induced by oncogene activation (e.g., *RAS*), inactivation of tumor suppressor genes or hypoxic signaling, is observed in a variety of cancers (reviewed in Ref. [13]). Alternatively and importantly, extreme overexpression of MET may occur as the result of genetic amplification, both in certain primary cancers, frequently of the gastrointestinal tract, or in tumors that have acquired resistance to targeted therapy to other oncogenic

RTKs [14,15]. Cancer cells harboring MET amplification acquire a MET-dependent phenotype for survival and growth [16,17] in which the aberrantly high levels of MET present in these cells cause ligand-independent receptor dimerization/activation and induce HGF/SF expression in stromal fibroblasts [18] creating a tumor microenvironment in which MET signaling drives invasion and metastasis. High expression of MET in colorectal, pancreatic, prostate, gastric, ovary or breast carcinoma is correlated with the development of metastasis and poor prognosis (reviewed in Refs. [3,6]).

The compelling evidence for a critical role of HGF/SF-MET signaling in humans has led to the recent development of a large number of MET kinase inhibitors [6] and antibodies acting on MET [19–24]. Nonetheless, several studies in which cancer patients received a MET antibody (onartuzumab) in addition to standard therapeutic regimens failed to improve clinical outcome in patient groups unselected for MET activity [25–29].

Two major lessons have been learned from these studies: (i) MET therapeutics clearly ought to be administered not to unselected populations but to patients in which the target is demonstrably a disease driver, and (ii) new classes of MET therapeutics are clearly needed, as resistance to MET kinase inhibitors develops rapidly [30] and the monovalent format of the antibody used in the clinical studies listed above (necessary in order to abolish native agonistic activity of the bivalent IgG [20,22,31]) is not the most active and effective therapeutic format.

Designed ankyrin repeat proteins (DARPins) represent a promising alternative to antibodies as protein therapeutics [32,33]. The DARPin scaffold possesses exceptionally favorable biophysical properties, enabling efficient selection of highly specific and potent binders to virtually any target from large synthetic libraries. Furthermore, DARPins tolerate extensive protein engineering and can therefore be used as building blocks for the generation of more complex, multi-specific or functionalized binding agents [32]. While bispecific DARPins are easily constructed [32], and binders against the soluble ligand (HGF/SF) have been described as bispecific molecules together with a vascular endothelial growth factor (VEGF)-binding module [34], the binding of two soluble factors by a bivalent DARPin offers no functional advantage over mixing two monovalent binders.

In contrast, bi- or multi-paratopic molecules directed to surface receptors can exploit more complex binding modes, beyond mere avidity effects [35–37]. In these cases, the bi-paratopic molecules act in a completely different way from the sum of their monospecific components and can lock domains of the cell surface receptor in an inactive conformation [35–37]. This is also mechanistically different from bispecific antibodies that combine MET binding with one arm and binding to a separate target with the second arm [10,19,23]. Bi-paratopic DARPins instead bind MET receptors with both arms and may effectively block signaling as a result. Furthermore, DARPins directed to the MET receptor, unlike ones directed to the ligand, may have therapeutic activity in a number of cancers in which aberrant MET expression and signaling is ligand-independent.

The extracellular portion of the MET receptor is composed of several domains. N-terminally, the Sema domain, a seven-bladed β-propeller fold, contains a furin cleavage site between residues 307 and 308 [38]. The mature form of the MET receptor is cleaved by furin into a disulfide-linked heterodimer of a longer membrane-spanning β-chain of 145 kDa and a shorter, exclusively extracellular 50 kDa α-chain. Following the Sema and a small cysteine-rich domain (PSI), four subsequent immunoglobulin-like folds, named IPT1–4, form a stalk structure that holds the propeller domain in the correct orientation for ligand binding (reviewed in Ref. [3]).

Several fragments of the MET ECD have been produced using suitable mammalian expression systems [39] and have been used here in order to select a diverse set of highly specific MET-binding DARPins. These, in turn, have been used as building blocks to construct bi-paratopic molecules for elucidating the relevance of targeting particular epitopes on the MET ectodomain for inhibiting cellular signaling. Bi-paratopic DARPins thus provide a basis for a new class of promising MET inhibitors, whose mechanism of action we describe.

Results

Selection of specific binders to diverse epitopes on the MET ECD by ribosome display with domain direction

We used the DARPin technology and ribosome display selection from large synthetic libraries to generate a highly diverse set of binders to different regions of the MET ectodomain. For this purpose, we used libraries of different DARPin formats, conducted parallel selections using differently truncated MET proteins and domain-directed competition steps in order to ensure selection of binders to the different MET domains. A large number of initial binders were reduced to a core set using the following criteria: (i) after initial screening, flow cytometry was used in order to select DARPins binding native MET receptor on human cells, (ii) the cell-binding DARPins were filtered with respect to their binding affinity and monodispersity in solution, and finally, (iii) the latter were clustered in epitope binning and competition experiments (Supplementary Materials and Methods, Figs. S1 and S2).

Three constructs of the MET ectodomain were used as targets: The first, MET_{567}, comprises the N-terminal β-propeller fold (Sema domain) and the adjacent small

cysteine-rich domain (PSI). MET_{741} contains, in addition to MET_{567}, the IPT1 and IPT2 domains, whereas MET_{928} also comprises IPT3 and IPT4, representing the entire extracellular portion of the receptor (Fig. 1a). These truncation constructs allowed us to direct the selection process toward desired regions by using shorter constructs in a pre-panning step prior to the actual panning (Fig. 1b). This strategy favored the enrichment of variants binding to the epitopes present exclusively in the chosen target, as shown schematically in Fig. 1c.

Several synthetic libraries of DARPins in four different formats were employed for binder selection by ribosome display on the target MET constructs. Out of these four, two represent classical DARPin library formats with two or three internal repeat modules (N2C and N3C), respectively, with each repeat holding six randomized positions. The internal repeats are shielded on the N- and C-terminal side by capping modules derived from natural ankyrin proteins [40]. Two further libraries used here represent LoopDARPins [41], a modified format of the DARPin scaffold where an additional elongated loop was introduced into the β-turn connecting two of the internal repeat modules, thereby creating a more convex binding surface, in contrast to the concave interface of the classical DARPin. LoopDARPins have been shown to expand the range of possible epitopes that can be targeted by DARPins [41]. The LoopDARPin libraries used here (N3LC and Nr3LCr) both hold three internal repeats, whereas Nr3LCr possesses additional randomized positions in the capping repeats: two in the N-terminal and five in the C-terminal module.

Twelve parallel selections (Fig. S1, Table ST1), each comprising four cycles of panning and domain-directed enrichment (where applicable), yielded 130 different

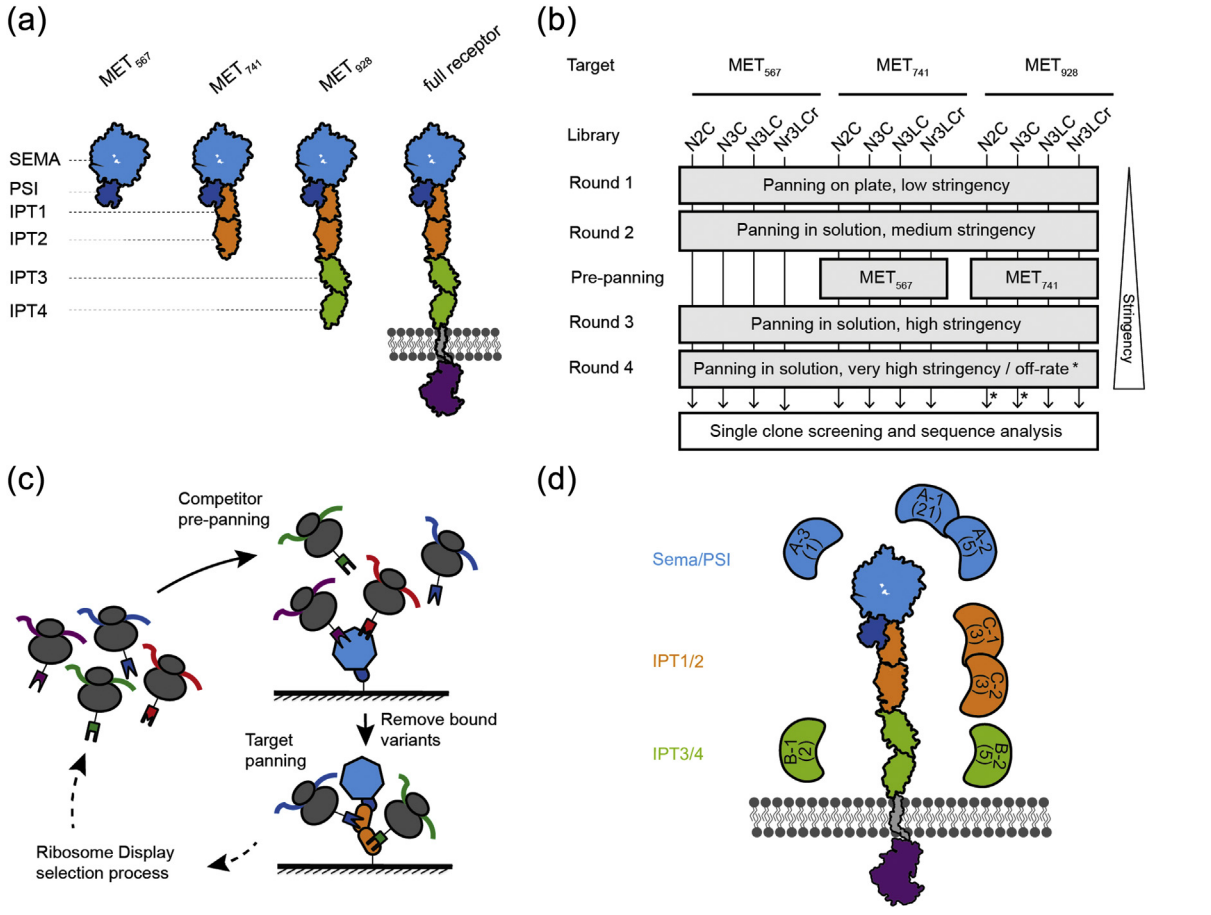

Fig. 1. Schematic representation of the selection process, used target constructs, DARPin libraries and identified epitope groups. (a) Schematic representation of MET ectodomain target constructs, (b) ribosome display selection workflow, (c) epitope direction strategy by pre-panning and (d) identified epitope groups. Receptor domains and binder groups are color-coded according to the targeted domains. Binder groups are labeled by group ID, and the number of binders in the respective group that have been investigated in detail is shown in parentheses.

DARPins that were tested for specific binding on MET-overexpressing cells by flow cytometry (Fig. S2d). Fifty binders showed clear and specific binding to native, membrane-bound MET as assessed by competition with unlabeled DARPin, and these were further characterized by epitope binning studies. DARPins binding to the same domain were tested in a cross-competition ELISA, which identified seven distinct subgroups (bins) (Fig. 1d and Fig. S2a–c). All DARPins binding to MET on cells were additionally analyzed for monodispersity in solution by size exclusion chromatography and were further ranked by time-resolved fluorescence resonance energy transfer (TR-FRET), allowing for additional clustering within the larger epitope bins (Fig. S2e and f).

Binding affinities of a subset of binders to all three targets were determined by surface plasmon resonance (SPR) with immobilized biotinylated MET_{567}, MET_{741} and MET_{928} and gave affinities in the high picomolar to low nanomolar range (Table ST2). For DARPins binding to the Sema (or PSI) domain, we found that their dissociation constants (K_D) differed by a maximum of a factor of two, when their binding to the three different target constructs was compared. This indicates that the epitopes involved are equally structured and accessible in the three MET constructs. The only exception is the binder G5A, whose epitope may bridge Sema/PSI and IPT1, resulting in about 3- to 4-fold higher affinity for MET_{741} and MET_{928}, compared to MET_{567}. DARPin C2C, initially assigned as an IPT1/2 binder, likewise displayed partial binding to MET_{567} and, like G5A, might bind to the interface region between Sema/PSI and IPT1. A2C, on the other hand, showed no binding to MET_{567} and bound IPT1 or IPT2 with a K_D of about 20 nM. All DARPins initially assigned as IPT3/4 binders indeed only interacted with MET_{928} with affinities in the higher picomolar to low nanomolar range.

Combinatorial screening revealed bi-paratopic DARPins with anti-proliferative activity on *MET*-amplified gastric cancer cells

We used the *MET*-amplified gastric carcinoma cell lines SNU-5 and KATOII, which display constitutive phosphorylation of the tyrosine residues responsible for kinase activation (Tyr1234/1235) (Supplementary Materials and Methods, Fig. S3) and depend on MET signaling for survival and growth [42], in order to test the biological activity of selected monomeric DARPins. We did not observe any change in cell proliferation upon treatment with individual MET-binding DARPins, as measured in the XTT assay (Supplementary Materials and Methods, Fig. S4). Previous work on HER2-addicted cancer cells, however, had revealed that covalent linking of two DARPins lacking activity as monomers resulted in bi-paratopic molecules capable of inhibiting growth and triggering apoptosis in the cancer cells [37].

On the strength of these results, we set out to explore whether homo-bivalent or bi-paratopic MET-binding DARPins could behave as effective and specific receptor antagonists. We generated bivalent and bispecific molecules with all two-DARPin combinations out of a core set of eight binders to different epitopes on the MET ECD using either a 5-amino-acid linker (termed L1) or a longer 20-amino-acid (termed L2) glycine–serine $(G_4S)_4$ linker (Fig. S5).

Next, all homo-bivalent or bi-paratopic DARPins were expressed in 2 ml *Escherichia coli* cultures, purified and tested for their ability to inhibit proliferation of the gastric adenocarcinoma cell lines SNU-5 and KATOII in the XTT cell viability assay.

Figure 2 depicts the result of the screening in a heatmap representation, revealing specific and consistent patterns of inhibited cell proliferation. From the constructs with the long linker, we identified highly distinct and robust inhibition for two molecules, the stronger of which was A3A–L2–A2C. This molecule binds to the Sema domain (A3A) on one side and to IPT1/2 (A2C) on the C-terminal side and inhibited the growth of SNU-5 and KATOII cells by 60%–70% and 30%, respectively. Construct A3A–L2–C3C on the other hand, binding to two different epitopes on the Sema domain, caused an inhibition of about 30% on SNU-5 and about 20% on KATOII. The experiments with the short-linked constructs confirmed the inhibitory activity of the A3A–A2C and A3A–C3C pairs and yielded additional candidates in which the N-terminal A3A domain was paired with the IPT1/2 binder C2C (70% inhibition on SNU-5 and about 25% on KATOII) or with the Sema binder C4A (30–40% inhibition on SNU-5, 10% inhibition on KATOII).

In general, the constructs with short linkers were less active at the lower of the two DARPin concentrations tested and interestingly, all bi-paratopic DARPins with growth-inhibitory activity contained A3A on the N-terminal side—a DARPin recognizing a unique epitope on the Sema domain (Fig. S2a)—connected to a second and different Sema binder (C3C, C4A) or to an IPT1/2 binder (A2C, C2C). The A3A epitope was defined further by crystallography (see below).

Two final points are noteworthy: the growth inhibition of selected bi-paratopic DARPins clearly exceeded the activity of the scFv 5D5 (Figs. 2 and 3, right panels), the precursor of MET-specific antibody onartuzumab [20], and all bi-paratopic DARPins tested failed to stimulate the proliferation of target SNU-5 and KATOII cells in the range of concentrations studied.

Activity of lead bi-paratopic DARPins depends on bispecificity and orientation

In order to validate the activity of the variants identified in the combinatorial screen, we produced several constructs on a larger scale and performed dose–response analyses. We also generated

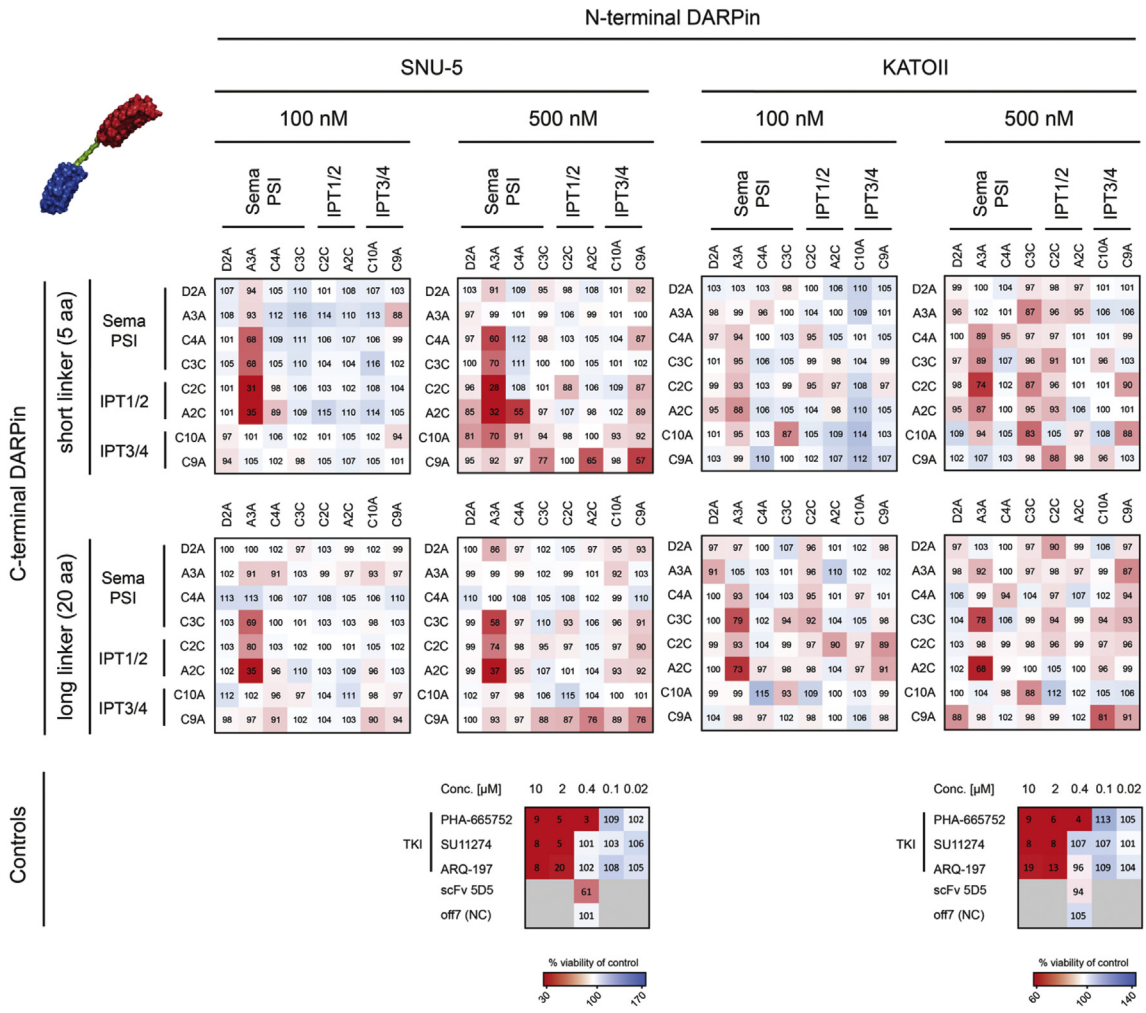

Fig. 2. Combinatorial screening of bi-paratopic DARPins reveals specific constructs with anti-proliferative activity on *MET*-amplified gastric carcinoma cells SNU-5 and KATOII. The model on the top left of the panels depicts two DARPins connected by a 20-amino-acid flexible linker. An N-terminal N2C DARPin is shown in blue, the linker in green and a C-terminal N3C DARPin in red as an example. The combinatorial screening for changes in cell proliferation by XTT assay is shown in a heatmap representation based on triplicate proliferation measurements as a percentage of non-treated controls. The resulting patterns are shown for SNU-5 cells on the left and for KATOII on the right. The top panels correspond to the treatment with DARPin–DARPin fusion constructs bearing a short (5-amino-acid) linker, and lower panels show the corresponding data for the constructs with a long (20-amino-acid) linker. Each grid of molecules was tested at a final concentration of 100 nM (left) and 500 nM (right). Controls for selective tyrosine kinase inhibitors (TKI), scFv 5D5 and the MBP-binding control DARPin Off7 are shown on the right. The color scheme was set to a range from 30% (red) to 170% (blue) relative proliferation for SNU-5 cells and from 60% (red) to 140% (blue) for KATOII cells, with white indicating no change in proliferation compared to the control.

constructs in which one of the MET binders was replaced by the MBP-binding DARPin off7 [43] as a negative control and additional ones in which the position in the construct of the two MET-binding DARPin was swapped. All of these control constructs were tested in both linker formats (L1, L2).

The bi-paratopic DARPins with growth-inhibiting activity yielded typical sigmoidal dose–response behavior with a robust plateau for the maximum cytostatic effect and IC_{50} values in the lower nanomolar range. Constructs A3A–A2C and A3A–C3C showed a slightly more potent response when connected by a long linker (20 amino acids, termed L2) in terms of both IC_{50} and maximal activity on SNU-5 cells (Fig. 3, upper left panel). The A3A–C2C and A3A–C4A constructs instead displayed stronger inhibitory activity when connected with the short linker (5 amino acids, termed L1) (Fig. 3, lower left panels). Importantly, none of the monovalent control constructs in which one binder was replaced by the non-binding control DARPin off7 showed activity (Fig. 3, upper right panels), and the effect of the inhibitory pairs was fully

dependent on the position of the two binding domains in the constructs, as confirmed by the lack of activity of constructs in which the arrangement of the two domains was reversed (Fig. 3, lower right panels). Also, scFv 5D5 was less potent in terms of IC_{50} or plateau reached.

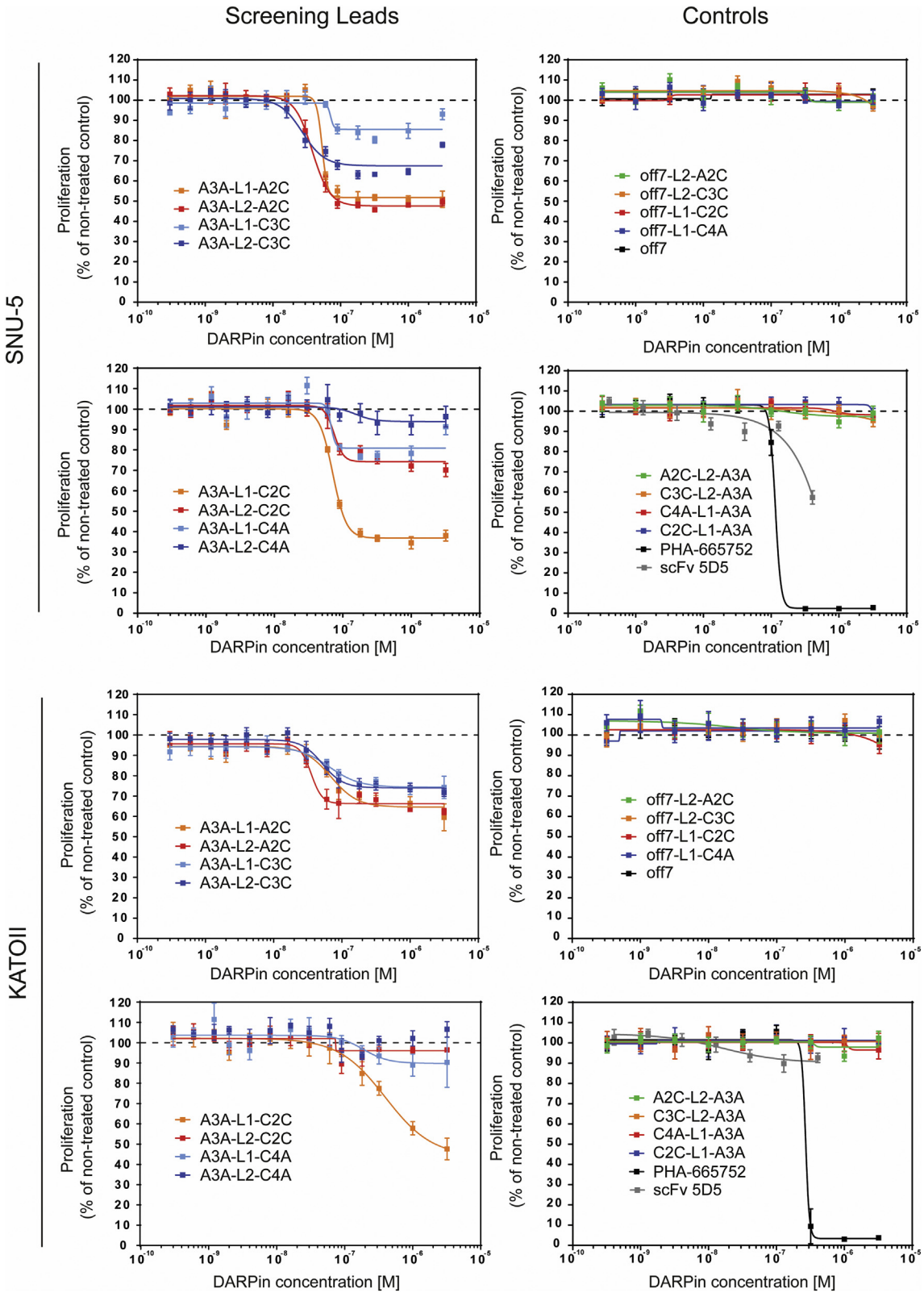

Active bi-paratopic DARPins possess a binding mode similar to HGF/SF

In order to gain further insight into the interaction between the DARPins contained in the bi-paratopic lead candidates and the MET ECD, we performed SPR measurements to monitor the binding in the presence of two MET ligands as competitors which have well-characterized binding interfaces: (i) the β-chain of mature HGF/SF, a serine protease homology domain, binding to blades 2 and 3 at the bottom face of the 7-bladed β-propeller that makes up the Sema domain (Fig. 4c, e) [44], and (ii) the bacterial invasion protein Internalin B (InlB), a protein of *Listeria monocytogenes* that promotes bacterial internalization into hepatocytes and epithelial or endothelial cells through the MET receptor, interacting with the MET IPT1 domain and blades 4 and 6 of the Sema domain [45] (Fig. 4). We used the fragment K4SP of HGF/SF, comprising the serine protease homology domain and the adjacent K4 (Kringle 4) domain and the MET-binding, N-terminal fragment $InlB_{321}$ of Internalin B in competition experiments with monovalent MET-binding DARPins.

The binding of K4SP was inhibited by prior binding of A3A but was not competed by the binding of the other three DARPins (Fig. 4a, top panels). Binding of $InlB_{321}$, on the other hand, was inhibited by prior binding of C3C, and to a slightly lesser extent after binding of C2C. DARPin A2C generated a very low response by itself, and therefore, the corresponding profiles do not enable any conclusions. These measurements indicated (i) overlap of the MET epitopes recognized by A3A and the β-chain of HGF/SF, (ii) overlap of the epitope recognized by C3C (a Sema binder) and the interrepeat (IR) region of $InlB_{321}$ [45] (Fig. 4b–e), and (iii) overlap of the epitope recognized by C2C (an IPT1/2 binder) and the leucine-rich repeat region of $InlB_{321}$ [45,46].

Further characterization of the A3A epitope was obtained via a crystal structure of A3A bound to MET_{741} in complex with $InlB_{321}$. We included $InlB_{321}$ as it may promote crystallization of the MET ECD by reducing inter-domain flexibility in MET through simultaneous interactions with both the Sema and the IPT1 domain [45]. Crystals of the A3A/MET_{741}/$InlB_{321}$ complex diffracted to 6-Å resolution (Table ST3) and a homology model of A3A could unequivocally be placed in the electron density (Table ST4; details how the position and orientation of the DARPin could be ascertained and rigorously verified in the crystal structure are provided in Materials and Methods).

In the crystal lattice, each A3A DARPin contacts two MET molecules. The smaller interface with the Sema + PSI domains involves mostly conserved residues of the DARPin scaffold, and we consider this to be a crystal packing contact (Figs. S6 and S7). The larger interface to the Sema domain represents the typical interaction between DARPins and their target molecules and involves many randomized DARPin residues or DARPin residues that were mutated during the selection process (Figs. S6 and S7), and we consider this to be the biologically relevant contact (Fig. 4). The final model after rigid body refinement resulted in plausible intermolecular contacts between A3A and MET.

The structure showed that A3A binds to the bottom face of the Sema propeller overlapping the MET epitope recognized by the β-chain of HGF/SF (Fig. 4b–e). The N-terminus of A3A points toward the adjacent PSI domain, whereas the C-terminus points away from the receptor. In principle, for a flexibly linked fusion of A3A to C3C—the latter presumably binding to blade 5 of the Sema domain since it clashes with the IR domain of $InlB_{321}$—intramolecular binding to one receptor would be conceivable. In the case of A3A–L1–C2C, however, given the short 5-amino-acid linker, intramolecular binding would only be possible in a hypothetical, very much strained tethered conformation of the MET ECD, where the Sema domain would have to be considerably bent toward the IPT stalk.

Bi-paratopic DARPins induce MET internalization, dephosphorylation and degradation and inhibit downstream signaling via Akt and Erk1/2

We investigated whether the inhibitory effects of bi-paratopic DARPins cause alterations in MET levels, MET activation and downstream signaling by Akt and Erk1/2, using Western blot analyses of SNU-5 and KATOII lysates after DARPin treatment for 48 h in the absence or presence of HGF/SF.

Treatment with the bi-paratopic DARPins caused a marked decrease in total MET receptor levels (Fig. 5). This reduction is more pronounced for constructs A3A–L2–A2C, A3A–L2–C3C and A3A–L1–C2C (up to 40%–50% decrease) than for A3A–L1–C4A and is not affected by the presence or absence of HGF/SF.

Next, we assessed phosphorylation at two essential phospho-tyrosine sites. Tyr1234/1235 is close to

Fig. 3. Activity of lead bi-paratopic DARPins is dependent on bispecificity and orientation. Validation and full dose–response curves of identified active bi-paratopic anti-MET DARPins by proliferation assays (XTT). Means and standard deviation of six biological replicates as percent of a non-treated control are plotted as a function of concentration of bi-paratopic or control DARPins on SNU-5 (top panels) and KATOII cells (bottom panels). Solid lines are obtained by fitting of a nonlinear regression function to data points in *GraphPad* software (log inhibitor *versus* response, variable slope, four parameters).

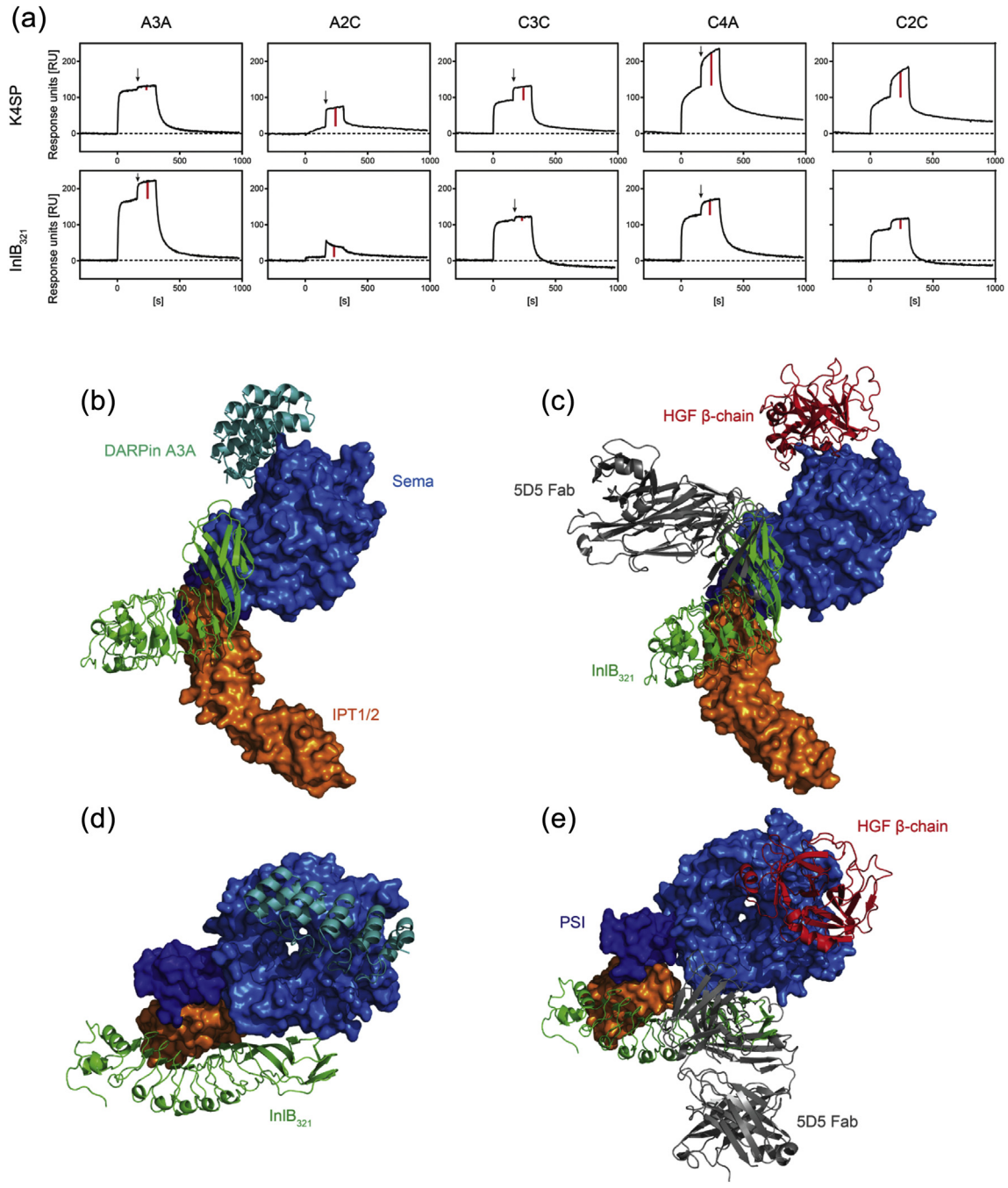

Fig. 4. Epitope characterization of DARPins contained in the bi-paratopic lead constructs. (a) SPR response traces are shown for injections of DARPins, each followed by a DARPin:K4SP (top row) or DARPin:$InlB_{321}$ (bottom row) mixture, indicated by arrows. The red bars illustrate the additional response by K4SP or $InlB_{321}$. (b, d) Crystal structure of the MET_{741}–A3A–$InlB_{321}$ complex (this work). (c, e) As a reference, the superimposed structures of MET_{741} in complex with $InlB_{321}$ from PDB entry 2UZY [45] with the HGF/SF β-chain from the complex structure 1SHY [44] and the onartuzumab (5D5) Fab from the complex structure 4K3J [31] are shown. Ligands (DARPin, HGF/SF β-chain, onartuzumab Fab and $InlB_{321}$) are shown in cartoon representation, and MET_{741} is shown in surface representation with Sema domain in light blue, PSI domain in dark blue and IPT1/2 in orange. Pictures were prepared with PyMOL software (DeLano Scientific LLC, Schrödinger).

the active site of the kinase domain, while Tyr1349 forms upon phosphorylation a bidentate docking site for several downstream signaling molecules (e.g., PI3K, PLCγ, Src, Shp2) as well as for the adaptor protein Gab1 [3]. We observed a diverging behavior of the four bi-paratopic DARPins tested.

DARPin constructs that contain a module that binds to the MET IPT1/2 domains (A3A–L2–A2C and A3A–L1–C2C) consistently led to a reduced phosphorylation signal, by at least the same extent as that of total MET. This therefore reflects a decrease of overall receptor. In the case of A3A–L1–C2C (Fig. 5b), additionally phosphorylation at Tyr1349 was almost completely abolished (reduced to 10%–15% of the initial level) in KATOII cells.

On the other hand, the constructs interacting with the Sema domain of MET with both binding modules (A3A–L2–C3C and A3A–L1–C4A) revealed no reduction or even considerable stimulation of MET phosphorylation at Tyr1349 in both cell lines.

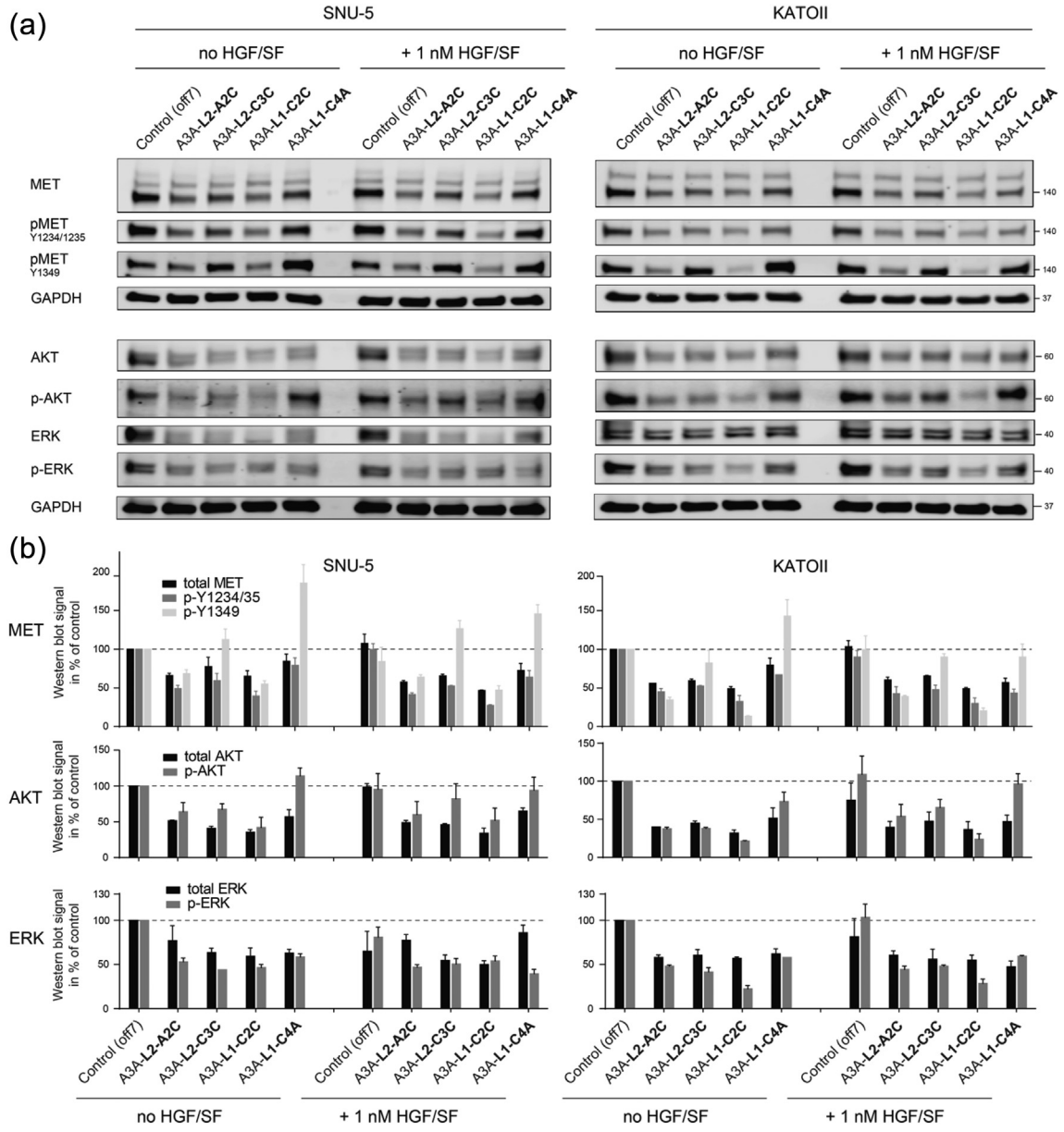

Fig. 5. Active bi-paratopic anti-MET DARPins lead to MET downregulation and inhibition of downstream signaling to Akt and Erk1/2. Western blot analysis of total levels and phosphorylation of MET, Akt and Erk. Representative membranes from three biological replicates. Whole-cell lysates were adjusted to equal concentrations of total protein, separated by SDS-PAGE and transferred to blotting membranes. Proteins and phosphorylation status were detected by specific primary antibodies, followed by fluorescently labeled secondary antibodies. (a) Signals were recorded on a fluorescence scanner. GAPDH was detected as a loading control. (b) Signals were quantified in *ImageStudio* software and normalized to the non-treated control (off7). Means from two biological replicates were plotted as histograms with standard deviations as error bars.

Considering the decreased receptor levels, this reflects a substantial gain in *relative* Tyr1349 phosphorylation per remaining receptor molecules. Treatment with A3A–L1–C4A of both cell lines led to a strong increase of the initial Tyr1349 phosphorylation, attenuated in part by addition of HGF/SF, indicating partial competition for MET binding (Fig. 5b). The MET-selective tyrosine kinase inhibitor PHA-665752 led to an almost complete abrogation of total MET levels as well as Tyr1234/1235 and Tyr1349 phosphorylation on both cell lines (Fig. S8).

Total Akt levels were reduced after DARPin treatment as well as after direct inhibition of the MET kinase by PHA-665752, in which case Akt levels are almost completely abolished (Fig. S8). Proteasome- or caspase-dependent degradation of Akt has been reported before in vascular smooth muscle cells following stimulation with platelet-derived growth factor (PDGF) or insulin-like growth factor-1 (IGF-1) [47], or in endothelial cells upon inhibition of vascular endothelial growth factor receptor (VEGFR) [48]; however, the function and detailed mechanisms of these processes remain largely unclear. In our studies, the overall decrease of total Akt closely reflected the treatment-induced decrease in level of MET receptor and phosphorylation caused by the respective constructs, resulting in a reduction between 40 and 70%. Phosphorylation at Ser473 of Akt, one of the two phospho-sites relevant for full Akt activation [49], revealed a similar pattern, whereas it was slightly less reduced upon DARPin treatment on SNU-5 cells as compared to KATOII. As seen for MET phosphorylation at Tyr1349, we observed *increased* Akt phosphorylation relative to total Akt levels after treatment with construct A3A–L1–C4A on both cell lines. In KATOII cells, effects on Akt phosphorylation were slightly diminished in the presence of HGF/SF, with the exception of A3A–L1–C2C, which maintained low Akt level and phosphorylation of 20%–30% of the control values.

Total Erk levels were considerably reduced upon treatment with the majority of DARPins and—to an even larger extent—after treatment with the kinase inhibitor PHA-665752 (Supplementary Materials and Methods, Fig. S8) and in SNU-5 cells, Erk downregulation was attenuated in the presence of HGF/SF. Levels of phosphorylated Erk were reduced by 40%–50% for most constructs on both cell lines and by 70%–80% for A3A–L1–C2C on KATOII. Together these studies indicated construct A3A–L1–C2C as the most potent inhibitor of MET-induced signaling and cellular proliferation in the *MET*-dependent gastric carcinoma cell lines.

Finally, we performed an internalization and degradation assay using a stable Flp-In TREx HEK293 cell line, in which overexpression of human MET, bearing an N-terminal HaloTag flexibly fused to the receptor α-chain, can be induced by tetracycline analogs. We recently developed an approach, in which we first label the HaloTag with a membrane-impermeable and then with a membrane-permeable fluorophore. This strategy allows us to quantify both cell surface and internal receptor levels by flow cytometry and thus monitor receptor internalization as well as receptor degradation [50]. Figure 6 shows the relative internal and surface MET levels as a function of time from 30 min to 24 h after treatment with 100 nM DARPin. In the absence of DARPins, about 80% of total MET-Halo was found inside the cells, likely at least in part a result of the N-terminal extension of the α-chain. Recently, a link between MET overexpression and its aberrant activation in the Golgi apparatus was shown, suggesting that non-canonical interactions between MET and other RTKs occur during maturation of receptors [51]. Upon treatment with bi-paratopic anti-MET DARPins, a considerable further decrease in both surface and internal receptor was found, and for all constructs, a reduction of surface MET of 40%–65% occurred in the first 30 to 60 min. The internal fraction also decreased significantly (30%–40%) after treatment with the active constructs between 8 and 24 h, presumably via degradation of MET.

The two bi-paratopic DARPins which, in addition to containing a Sema domain binder, carry an IPT1/2 binding module (A3A–L2–A2C and A3A–L1–C2C) showed the strongest activity, inducing MET internalization and degradation. This was stronger than the Sema–Sema binding constructs: the Sema–IPT1/2 linking DARPins caused sustained receptor downregulation after 24 h, whereas the Sema–Sema linking DARPins (A3A–L2–C3C and A3A–L1–C4A) revealed a slight rebound effect on surface MET levels after 6 to 24 h of treatment. The control DARPin A3A–L2–off7 (which binds monovalently to the Sema domain), as well as the monomeric control DARPin off7 (which does not bind at all) revealed no significant changes in MET receptor levels, internalization or degradation.

Discussion

A large body of evidence has accumulated over three decades identifying the MET receptor and its ligand HGF/SF as a signaling system crucially involved in cancer development, progression, invasiveness and metastasis (reviewed in Refs. [3,6,52]). As a therapeutic target, however, MET has posed fundamental challenges, demonstrated by the fact that to date no selective inhibitor of MET or HGF/SF—small-molecule or antibody—has shown sufficient benefit and efficacy for clinical approval.

At least eight MET-specific monoclonal antibodies have been or are currently tested in clinical trials (recently reviewed by Kim and Kim [53]). Several of them induce receptor dimerization and possess considerable agonistic activity requiring re-engineering the

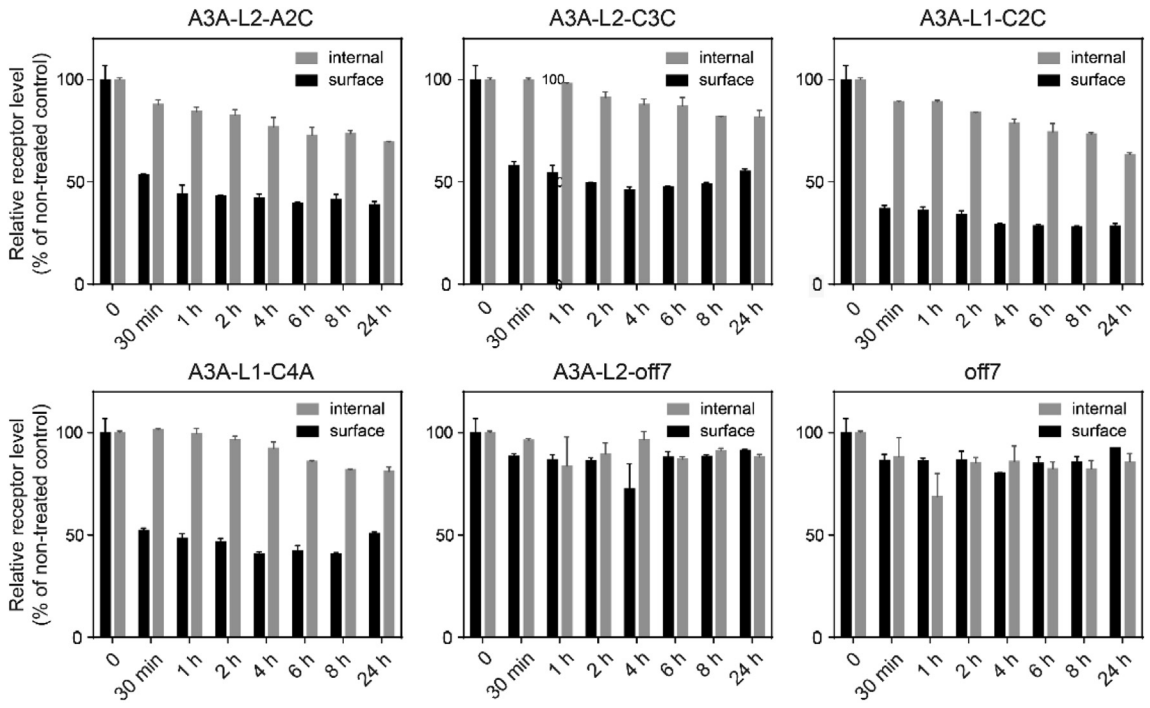

Fig. 6. Active bi-paratopic DARPins lead to MET receptor internalization and degradation. Internalization and degradation assay using HEK293 cells inducibly expressing MET-HaloTag fusions, and sequentially stained with a membrane-impermeable and a membrane-permeable fluorescent HaloTag ligand. Cells were induced for MET-Halo expression 24 h prior to the experiment. After DARPin treatment at several time points, cells were sequentially stained with AF660- and TMR-containing HaloTag ligands, fixed, and fluorescence was measured by flow cytometry. Duplicate signals were normalized to the respective non-treated control values and plotted with error bars representing the standard deviation.

antibody to a monovalent format, as carried out with onartuzumab (MetMAb) [31]. A recent patent application [57] described another yet unpublished approach, where IgGs that display some growth inhibitory effect were used to construct more potent bispecific anti-MET antibodies. Growth inhibition was observed especially with Hs746T cells which carry a mutation in the *MET* gene that removes the juxtamembrane domain [58]. To judge the general activity and usefulness of these antibodies in cancer therapy further studies will be required.

PHA-665752 was described as a potent and selective competitive inhibitor of the MET kinase [54] and is a valuable research tool, but it is not one of the relatively few small molecule MET kinase inhibitors currently in clinical trials [55]. While the activity of these molecules is strong (Fig. S8), small-molecule inhibitors of the MET kinase have shown considerable levels of off-target effects [56] and typically lead to the emergence of resistance in cancer cells [30]. These findings clearly demonstrate the need for novel formats and approaches in the field, as well as mechanistic investigations into modes of action of inhibition, which is where the work described here seeks to contribute. We built on the demonstration that certain RTKs can be inhibited by bi-paratopic binding agents that lock the ECDs of the receptor in a signaling-incompetent conformation. For instance, bi-paratopic DARPins binding to ErbB2 induce apoptosis and have strong in vivo anti-tumor effects on ErbB2-dependent cancers [36,37]. Similarly, bi-paratopic DARPins targeting EGFR inhibit proliferation of EGFR-overexpressing cells [35].

Here we demonstrated that this conceptual approach can be extended to MET, an RTK of a different family, and we described the steps necessary to achieve this result. Flexibly linked DARPins binding to a receptor may display several different modes of action. First, such molecules could exert agonistic activity by crosslinking MET receptors to active dimers competent for downstream signaling. Second, they could act as a true ligand-antagonist by blocking the interaction of MET with HGF/SF. Or, third, they could lead to a trapping of receptors in an inactive conformation by either intra- or intermolecular cross-linking of MET ECDs, independent of the MET ligand. In addition, interaction with the DARPins could induce receptor internalization. It is important to understand that only the latter mode of action might be able to inhibit MET signaling in cancer cells—such as SNU-5 and KATOII in which MET signaling is ligand-independent.

Following ligand-induced activation, receptor internalization represents the first step in a series of events

which is frequently used by RTKs for temporal and spatial regulation and fine-tuning of ligand-induced signaling. It is conceivable that binding of A3A to the HGF/SF β-chain epitope on the bottom face of the β-propeller (Fig. 4) may play a pivotal role in triggering receptor internalization, which we have observed as a consequence of DARPin treatment. Binding of A3A to MET, however, is necessary but not sufficient in order to achieve MET downregulation, as our studies demonstrated a requirement for binding to a second separate binding site on the β-propeller or the IPT1/2 domains in order to achieve inhibition. This is directly confirmed by the lack of activity of the A3A–L2–off7 control construct (Fig. 6). These findings clearly demonstrate the necessity for a comprehensive screening for bi-paratopic constructs, as single monomeric DARPins upon binding to MET do not induce any effect on receptor signaling, a fact that could well be related to the nature of the MET receptor activation with its bi-paratopic ligand HGF/SF. The comprehensive analysis of the entire combinatorial space of a diverse collection of binding modules enabled us to identify the relevant specific epitope regions on the MET receptor as well as the geometric properties of such bi-paratopic binding molecules in a highly systematic manner.

We have obtained evidence that bi-paratopic binding is intermolecular. Kinetic binding curves of the bi-paratopic constructs show a biphasic dissociation behavior (Fig. S9a), but the dissociation rate constants are those of the constituent monomers (Fig. S9b), consistent with monovalent binding of either of the constituent DARPin units, and inconsistent with bivalent binding to the monomer. At the achievable densities of MET on the grating-coupled interferometry sensor surface, intermolecular binding is apparently not possible. In contrast, titration experiments with the bi-paratopic DARPins on KATOII cells (Fig. S9c) show a significantly improved apparent affinity (avidity) compared to the monomers, indicating that bivalent binding does occur on cells, where MET can be clustered, consistent with the biological effects that were only observed with bi-paratopic constructs.

Our study focused on the two carcinoma lines with amplified *MET* locus (SNU-5 and KATOII) because such tumors are proving highly refractory to the therapeutics currently available. In parallel studies on lung (A549) and ovarian (SKOV-3) carcinoma lines responsive to HGF/SF, we observed no measurable growth response to the physiologic MET ligand (Fig. S10) but a significant motility response (Fig. S11a). Some anti-MET DARPins had weak but measurable agonistic activity on A549 and SKOV-3 cells (Fig. S11b), and the most active inhibitory ones reduced HGF/SF-induced motility by 50% to 75% (Fig. S11b and c).

In summary, the bi-paratopic DARPins described here constitute a new class of synthetic, high-affinity MET ligands that lack significant agonistic activity and define a new mechanism of receptor antagonism. This may find interesting applications in cancers in which the *MET* gene is amplified causing massive receptor overexpression and ligand-independent, constitutive MET signaling.

Materials and Methods

General materials

All chemicals and reagents were purchased from Sigma-Aldrich (Buchs, Switzerland) unless stated otherwise. Herculase II Fusion DNA Polymerase was purchased from Agilent (Santa Clara, USA). FastAP Thermosensitive Alkaline Phosphatase was obtained from Thermo Fisher Scientific (Rockford, USA). Restriction enzymes were from New England Biolabs (Ipswich, USA) or Thermo Fisher Scientific. T4 DNA Ligase was obtained from New England Biolabs. *E. coli* strain XL1 blue and strain BL21 (DE3) were purchased from Stratagene (Agilent).

Target proteins and DARPin libraries

Three constructs of the MET receptor ectodomain were used as targets for the DARPin selection by ribosome display. MET_{567}, MET_{741} and MET_{928} were expressed and purified as described elsewhere [39]. All three were chemically biotinylated at primary amines for target immobilization by standard NHS-chemistry.

The randomized N2C, N3C, N3LC and Nr3LCr DARPin libraries were amplified by PCR from the pRDV plasmid from master stocks using the oligonucleotides T7B (5′-ATACGAAATTAATAC-GACTCACTATAGGGAGACCACAACGG-3′) and tolAk (5′-CCGCACACCAGTAAGGTGTGCGGTTT-CAGTTGCCGCTTTCTTTCT-3′) to generate working stocks. All working stock aliquots covered at least twice the calculated practical diversity of the provided portion of the master stock in the volume used for the *in vitro* transcription reaction. *In vitro* transcription was performed for all libraries according to the standard ribosome display protocol [59], and aliquots of 10 μg input RNA were prepared and stored at −80 °C.

Ribosome display

In vitro ribosome display selections were conducted according to the standard ribosome display protocol for large libraries [59] and as previously described [43,60,61] with the following adaptations. All selections except the first round were performed in solution in 96-deep-well plates on the King-Fisher Flex (Thermo Fisher Scientific). Every selection cycle contained a 30-min pre-panning step on streptavidin-coated magnetic beads (Dynabeads

MyOne Streptavidin T1; Invitrogen, USA), a 1-h target binding step (panning) and a 30-min target pulldown step by streptavidin-coated magnetic beads. Selection stringency was increased by extended washing steps after target pulldown, lowered target concentrations (from 350 to 200 nM; 10 nM in off-rate selection rounds) and/or off-rate selection by competition with non-biotinylated target present in 315-fold molar excess. RNA isolation after selection rounds was performed with the SV Total RNA Isolation System (Promega). For reverse-transcription of purified RNA to cDNA the oligonucleotide JSCRDir2 (5′-ATCTGCTTCGGCCTTCGCTTTAGCATCTGCCGC CGCTTTCG-3′) was used. Oligonucleotides JSCRDir2 and JSCRDif4 (5′-AGAGGATCGCATCAC-CATCACCATCACGGATCCGACCTGGG-3′) were used for amplification of cDNA by PCR.

Analysis and ELISA screening of selection pools

After ribosome display selections, reverse-transcribed and amplified output sequences were subcloned into the expression vector pDST67, 95 to 190 single clones were isolated from each selection strategy and pellets of 1-ml expression cultures were lysed using 50 µl B-PERII (Thermo Fisher Scientific). Biotinylated target proteins (100 nM) in PBS-TB [PBS containing 0.1% (v/v) Tween-20 and 0.2% (w/v) BSA; pH 7.4] were immobilized on 384-well high binding microplates (Greiner Bio-One GmbH, Frickenhausen, Germany) previously coated with 66 nM streptavidin (Thermo Fisher Scientific) in PBS and blocked with 0.2% (w/v) BSA in PBS. Crude extracts of expressed DARPin clones were diluted in PBS-TB and applied to the wells with or without immobilized target for 60 min at RT. After repeated washing, bound DARPins were detected with an anti-RGS-His antibody (Qiagen GmbH, Hilden, Germany), a secondary anti-mouse-IgG-alkaline phosphatase conjugate (Pierce, Thermo Fisher Scientific) and *p*-nitrophenylphosphate (Sigma-Aldrich) as substrate. Sequencing of 4 to 28 clones with good ELISA signal/background ratio per selection pool was performed by standard Sanger sequencing at GATC (Konstanz, Germany).

Construction and purification of DARPins and DARPin fusions

Classical molecular cloning was used to generate all variants and fusions of DARPins. The DARPin sequences were subsequently introduced into the previously prepared respective plasmids pQiBi_01 or pQiBi_22 harboring the sequences for the flexible linkers L1 or L2, respectively, flanked by BamHI/HindIII (downstream) and BglII/BsaI (upstream) cloning cassettes. The plasmids are *lacI*^{q}-containing derivatives of the vector pQE30 (Qiagen).

Standard bacterial expression under control of a *lac* promotor was performed at different scales (1 ml to 1.5 L) for all DARPin constructs in this work using *E. coli* strains XL1 blue or BL21 in 2YT bacterial medium. Expression cultures were inoculated with a starter culture to an OD_{600} of 0.1–0.2 and grown for 4–6 h at 37 °C or overnight at 25 °C after induction with 0.5 µM IPTG (Sigma-Aldrich). For larger-scale cultures (>20 ml), cells were lysed mechanically by classical French press or a continuous flow cell disruption system (Constant Systems Ltd., Northants, UK). For small-scale expressions (≤20 ml), cell lysis was performed mechanically on a small-scale continuous flow cell disruption system (in-house prototype) or chemically by Cell Lytic B Lysis reagent (Sigma-Aldrich). Cleared and filtered lysates of larger cultures were purified by His-tag immobilization on a Superflow Ni-NTA immobilized metal-ion affinity chromatography (IMAC) resin (Qiagen), several washing steps and elution with PBS containing 250 mM imidazole (pH 7.4). Lysates of smaller-scale cultures were purified via HisPur™ Cobalt Resin (IMAC) in 96-well format (Thermo Fisher Scientific). Buffer exchange and removal of imidazole were performed by dialysis or size exclusion/buffer exchange chromatography. All purifications of proteins subsequently subjected to assays on mammalian cells involved additional extensive washing on the IMAC resin with 60–80 column volumes of washing buffer containing 0.5% (v/v) Triton X-114 (Sigma-Aldrich), followed by 50 column volumes of cell culture grade PBS (Sigma-Aldrich) for removal of bacterial endotoxins.

Flow cytometry

We used a Cyflow Space multi-laser flow cytometer (Sysmex Partec, Norderstedt, Germany) for detecting binding of His-tagged DARPins or DARPin-sfGFP fusions on MET-overexpressing cells. Cells (0.5–2 million) were incubated with 1 µM DARPins/DARPin fusions for 1 h at 4 °C in PBS–BSA (PBS, 1% BSA) and washed three times with cold PBS. For His-tag detection, the cells were incubated with an anti-penta-His antibody conjugated to Alexa Fluor 488 (Qiagen) for 1 h at 4 °C and washed again three times. Cells were resuspended in PBS–BSA immediately before the measurement. At least 50,000 cells gated for singlets and viability were used for analysis. For competition measurements, 0.5–2 million cells were pre-incubated with 1 µM DARPin at 4 °C, and 100 nM DARPin–sfGFP fusion was added after 1 h and incubated for another hour at 4 °C. Mean fluorescence intensity values of competition samples were compared to non-competed samples for analysis. All incubation steps were performed with PBS containing 0.1% (w/v) BSA. Data analysis was performed by FlowJo™ software (FlowJo, LLC, Ashland, USA).

For titration experiments with bi-paratopic DARPins, 100,000 KATOII cells were incubated with the respective DARPin concentration in PBS-BA

(PBS, 1% BSA, 0.01% sodium azide) for 1 h at 4 °C, washed three times with PBS and resuspended in PBS containing LIVE/DEAD™ Fixable Aqua Dead Cell Stain (Thermo Fisher Scientific). Cells were washed twice with PBS after 30-min incubation and fixed with 4% paraformaldehyde for 20 min. Fixation was quenched with PBS–BSA, and cells were washed three times and incubated with a polyclonal anti-DARPin rabbit serum (1:1000) in PBS–BSA for 1 h. The cells were washed three times, incubated with a secondary anti-rabbit APC-labeled antibody (1:1000) for 1 h, washed twice and fixed again for 20 min as described before. Staining was recorded on a BD LSR II Fortessa, and the mean fluorescence intensity values of viable singlet cells were plotted, normalized to the respective final plateau levels.

Epitope binning ELISA

Epitope binning competition ELISA was performed on 384-well high binding microplates (Greiner Bio-One GmbH) with immobilized biotinylated target proteins (MET_{567}, MET_{741} or MET_{928}) as described before. DARPins without HA-tag were applied to the wells in columns of the microtiter plates at 500 nM final concentration and incubated for 1 h at 4 °C. DARPins containing an additional C-terminal HA-tag were then added in rows of the plates to a final concentration of 50 nM and the plates incubated for another hour at 4 °C. After three washing steps, binding of HA-tagged DARPins was detected using an anti-HA antibody (Sigma-Aldrich), a secondary anti-mouse-IgG-alkaline phosphatase conjugate (Pierce, Thermo Fisher Scientific) and *p*-nitrophenylphosphate (Sigma-Aldrich) as a substrate. All buffers and further conditions were identical to the ELISA protocol described above.

Time Resolved FRET

TR-FRET measurements were performed as one-pot reactions using 1 nM biotinylated MET_{928} as target, 8 nM DARPin containing an N-terminal His_6-tag, 16 nM streptavidin-terbium-cryptate conjugate as FRET donor (Cisbio, Codolet, France), 16 nM anti-His_6 IgG conjugated to the dye d2 as FRET acceptor (Cisbio) and 100 nM non-biotinylated MET_{928} as competitor. Assays were conducted in white 384-shallow-well plates (Thermo Fisher Scientific), previously blocked with PBS containing 0.5% (w/v) BSA. Reactions were performed in PBS containing 0.2% (w/v) BSA. Signals were recorded in 7-min intervals immediately after the addition of competitor.

Kinetic measurements

SPR measurements with monomeric DARPins were performed on a ProteOn™ XPR36 system (Biorad, Hercules, USA). Experiments were performed in TBS_{150} containing 0.005% (v/v) Tween-20 at 25 °C. Biotinylated MET target proteins were immobilized in duplicate ligand channels on a ProteOn™ NLC sensor chip to 200–500 response units. For kinetic analysis, five concentrations of a dilution series of each DARPin in a range between 0.4 and 300 nM were injected for 300 s, and dissociation with buffer flow was followed for 5000 s. The signal from a buffer reference analyte channel was subtracted from the measurements, and signal from interspot reference positions was used to correct for bulk signal changes and baseline drifts. Association and dissociation rates were determined by global fitting of the signal profiles to a kinetic Langmuir model. In cases of poor fitting to the kinetic Langmuir model due to very fast association or dissociation, K_D values were assessed by an equilibrium binding model. In cases of very slow and incomplete dissociation between concentration steps, we applied a kinetic titration model [62].

For competition experiments, subsequent injections of a saturating concentration of 300 nM DARPin, well over the K_D, followed by a mixture of 300 nM MET ligand (K4SP, $InlB_{321}$) and 300 nM DARPin were performed, monitoring any further addition of SPR response units. Signal processing was done as previously described, and the response traces were evaluated with respect to additional signal by the MET ligands in the second injection.

Kinetic characterization of bi-paratopic DARPins was performed by grating-coupled interferometry on a Creoptix WAVE system (Creoptix AG, Switzerland), a label-free surface biosensor. MET_{741} target protein was immobilized on 4PCP WAVEchips (quasi-planar polycarboxylate surface; Creoptix AG, Switzerland) to a density of 1500 to 2000 pg/mm^2 by standard amine-coupling chemistry. A dilution series of DARPins (45 pM to 100 nM) was injected in duplicates for 200 s, followed by buffer injection for 400 s. All measurements were performed in PBS P+ [PBS, 0.005% (v/v) Tween-20]. Data were double-referenced by subtracting the signal of blank injections as well as the reference channel, corrected for small bulk refractive index mismatches and analyzed in WAVEcontrol software (Creoptix AG, Switzerland). A Langmuir 1:1 or a heterogeneous analyte model was used for data fitting.

Size exclusion chromatography

Analytical size exclusion experiments were performed with PBS as running buffer either on an ÄKTA Micro system using a Superdex-200 PC 3.2/30 column with a flow rate of 60 µl/min or on an Agilent HPLC system using a Superdex-200 Increase GL 5/150 column with a flow rate of 200 µl/min. Preparative size exclusion chromatography was performed on an ÄKTA Pure system using a Superdex 200 30/300GL column with a flow rate of 0.5 ml/min and HBS (Hepes buffered saline) as running buffer (all systems and columns from GE Healthcare, UK).

MET ligands, inhibitors and cell lines

The MET ligand HGF/SF and the ligand fragment K4SP were produced as previously described [63]. The scFv of the anti-MET antibody 5D5 [22], the precursor of onartuzumab [20], was expressed in CHO cells and purified from the supernatant by cation exchange chromatography (HiTrap CM FF; GE Healthcare) using a Bis–Tris buffer (pH 6.8) and subsequent Ni-NTA IMAC (HisTrap FF; GE Healthcare). Internalin B proteins $InlB_{241}$ and $InlB_{321}$ were produced as previously described [45]. MKN-45 cells were purchased from DSMZ (Braunschweig, Germany). SNU-5, KATOII and Okajima cells were kindly provided by M. Park (McGill University, Montreal, Canada). U87-MG and H1993 were purchased from ATCC (Manassas, USA). Tyrosine kinase inhibitors PHA-665752, SU11274 and ARQ-197 were purchased from Selleckchem (Houston, USA).

Cell proliferation assay

Formazan-based cell proliferation assays were performed using the Cell Proliferation Kit II (XTT) (Roche, Basel, Switzerland) or Cell Proliferation XTT Kit (NeoFroxx, Einhausen, Germany). For SNU-5 and KATOII cells, depending on the treatment time, 300 to 600 cells were seeded 24 h before treatment in 25 µl RPMI 1640 medium supplemented with antibiotics (penicillin/streptomycin) and 10% (v/v) fetal bovine serum from Amimed™ (Bioconcept, Allschwil, Switzerland) into Falcon™ clear TC-treated 384-well microplates (Corning, NY, USA). All pipetting steps involving 384-well plates were conducted with the semi-automated pipettor system CyBio™ SELMA (Analytik Jena, Germany). Treatments were applied with compounds diluted in PBS or HBS, adding 5 µl to the respective wells and incubating for 4 to 6 days. After treatment, 25 µl of XTT reagent solution 1:1 diluted with serum-free RPMI medium was added to the wells and the plates were incubated for 1 to 4 h at 37 °C for signal development. Absorption at 450 nm of developed plates was measured on a Tecan Infinite M1000 microplate reader (Tecan, Männedorf, Switzerland). Background signal of control wells without cells was subtracted from data prior to analysis.

Motility assay

Two human cell lines, the ovarian cancer SKOV-3 and the lung adenocarcinoma line A549, were routinely grown in RPMI 1640 with GlutaMAX medium (Life Technologies), supplemented with antibiotics and 10% (v/v) fetal bovine serum (Life Technologies). The cell migration assay was performed with both cell lines using a modified Boyden chamber (AC96 Migration Chamber, Neuroprobe) with a porous membrane (8 µm, PVP-free) previously coated with 100 µg/ml collagen (Purecol, Nutacon) in PBS. Cells were seeded in the top part of the chamber at a density of 10^6/ml resuspended in serum-free RPMI 1640 with 0.25% (w/v) bovine albumin. DARPins at selected concentrations, in the presence or absence of HGF/SF at 10^{-9} M, were added to the bottom part of the chamber. Cell migration was allowed to continue for 6 h at 37 °C in a 5% CO_2 incubator. After that, the apparatus was disassembled and non-migrated cells on the filter were gently removed by wiping the surface with cotton balls. Migrated cells on the filter were fixed for 1 h in 4% formaldehyde and stained for 30 min with green HCS Cell Mask Stain (Life Technologies) at 1 µg/ml. Fluorescence intensity was measured using a POLARStar Omega plate reader (BMG Labtech) using excitation/emission settings of 485 nm/520 nm, respectively. Background fluorescence from non-stimulated cells was subtracted, and the data shown are the means of three or more independent experiments.

Immunoblotting and antibodies

Two million SNU-5 or KATOII cells were seeded 24 h before treatment in RPMI 1640 medium supplemented with antibiotics and 10% (v/v) fetal bovine serum from Amimed™ (Bioconcept, Allschwil, Switzerland) to round 150-mm-diameter tissue culture dishes. For signaling experiments, cells were treated with 200 nM DARPin constructs or 1 µM tyrosine kinase inhibitor and/or 1 nM HGF/SF diluted in PBS for 48 h. Treated cells were harvested by centrifugation from the supernatant medium and by mechanical scraping from the plates in the presence of protease and phosphatase inhibitors [PBS (pH 7.4), 50 mM Na-fluoride, 1 mM Na-orthovanadate, 1 mM Na-metavanadate, 1 mM Na-molybdate, 1 mM β-glycerolphosphate, 1 mM Pefabloc, 10 µg/ml Pepstatin A, 10 µg/ml Leupeptin, 10 µg/ml Marimastat] on ice. Cells were washed once in cold PBS with inhibitors, resuspended in 50 to 200 µl lysis buffer (PBS with inhibitors and 1% Triton X-100) and lysed under extensive shaking on a tube rocker at 1200 rpm for 30 min at 4 °C. Lysates were cleared by centrifugation at 12,000*g* for 10 min, and supernatants were transferred to fresh tubes. BCA assays were performed for determining total protein concentrations, and the lysates were equally adjusted to 2–5 mg/ml total protein. Adjusted samples were denatured in the presence of reducing Laemmli buffer for 10 min at 80 °C and run on 4%–20% Mini Protean TGX™ polyacrylamide gels (Biorad) at constant 15 mA. Separated proteins were transferred to PVDF membranes (Immobilon-P 0.45 µm; EMD Millipore) using wet transfer at 100 V for 60 min. Membranes were blocked with PBS containing Sigma blocking solution (Sigma-Aldrich) for 20 min and incubated with primary antibodies in PBS-TB (PBS containing blocking buffer and 0.05% Tween-20) overnight at 4 °C. After four washing steps in PBS-T (PBS containing 0.05%

Tween-20), the membranes were incubated with secondary antibodies conjugated to IRDye 800CW or IRDye 680LT (LI-COR, Lincoln, USA) diluted 1:10,000 in PBS-TB for 1 h at RT. Membranes were washed again three times with PBS-T, and fluorescence was measured using a LI-COR Odyssey system. Image Studio software (LI-COR) was used for quantification of signal intensities.

Primary antibodies against all targets (except GAPDH loading control) were purchased from Cell Signaling Technology (Danvers, USA). The anti-GAPDH loading control antibody was purchased from Thermo Fisher Scientific. Secondary IRDye-conjugated antibodies were purchased from LI-COR.

Protein expression and purification for crystallization

DARPin A3A was expressed and purified as described above, MET_{741} and $InlB_{321}$ as previously described [45]. Prior to crystallization, all proteins from frozen stocks were analyzed for purity by SDS-PAGE and for monodispersity by gel filtration on a Superdex 200 10/300 column equilibrated in 10 mM Hepes (pH 7.5) and 150 mM NaCl. MET_{741} was further purified via size exclusion chromatography under the same conditions to remove aggregates.

Protein crystallization

MET_{741}, $InlB_{321}$ and DARPin A3A were mixed in equimolar ratio directly prior to setup of crystallization trials. Four hexagonal, rod-shaped crystals grew in 100 nl of MET_{741}–$InlB_{321}$–A3A complex at 5 mg/ml total protein concentration and 100 nl of reservoir solution E3 from the MbClass II Suite crystallization screen by QIAGEN [0.1 M Hepes sodium salt (pH 7.5), 12% w/v PEG 4000] in a sitting drop at 20 °C after roughly 1 week. Attempts to optimize these initial crystals or to improve diffraction properties by controlled dehydration failed. Crystals were cryo-protected in reservoir solution containing 20% glycerol and flash-cooled in liquid nitrogen.

Data collection, processing and structure determination

X-ray diffraction data were collected at beamline P13 operated by EMBL Hamburg at the PETRA III storage ring [64]. Two wedges from a single crystal were indexed and integrated separately with the XDS package [65] and scaled together with AIMLESS [66] from the CCP4 package [67]. The structure was solved by molecular replacement with Phaser [68]. Two copies of MET_{741} in complex with $InlB_{321}$ [Protein Data Bank (PDB) ID 2UZY] [45] were placed first. Then, individual domains or domain combinations were exchanged for higher resolution structures. The Sema domains were replaced by the Sema domain of PDB ID 1SHY [44], and PSI, IPT1 and IPT2 were replaced by those of PDB ID 5LSP [69]. Positions of all structural domains were refined in Phenix [70] as separate rigid bodies. Exchange of $InlB_{321}$ from PDB ID 2UZY against $InlB_{321}$ from higher-resolution structures PDB ID 1H6T or 2UZX did not improve *R*-factors and was, therefore, omitted. After rigid body refinement of MET and $InlB_{321}$ domains, there was clear difference density for the DARPin (Fig. S12). Phaser correctly placed a homology model of DARPin A3A that we generated according to the blueprint file (PDB ID 2XEE; [71]) into this density. Due to the limited resolution, only rigid body and grouped B-factor refinement were performed. This resulted in a good fit to the electron density (Fig. S13), reasonable *R*-factors and plausible intermolecular contacts except for severe clashes between residues Asp275, Phe238 and Arg310 from $InlB_{321}$ and residues Lys376, Met431 and Ser470 from MET_{741}. To generate a physically more realistic model, we chose other rotamers in Coot [72] for $InlB_{321}$ residues Asp275, Phe238 and Arg310 as well as for MET_{741} residues Lys376 and Met431. Data collection and refinement statistics are reported in Table ST3.

Despite the low resolution of the data, the DARPin could be oriented and positioned unequivocally. Due to its inherent asymmetry (curvature in two directions and presence of long loops on only one side), it is almost impossible to orient the DARPin wrongly in the electron density. We intentionally tried to manually misorient the DARPin by rotating it roughly 180° around one of several axes and moving it into density in the program Coot or followed by rigid body refinement. All our attempts, however, resulted in an unsatisfactory fit to the electron density and in a substantial increase of R_{free} (not shown). Shifting the register of the DARPin by one repeat unit toward the N- or C-terminus resulted in a satisfactory fit to the electron density for all repeats but one. We performed these register shifts toward the N- or C-terminus for both DARPins in the asymmetric unit and calculated *R*-factors and electron density for five iterations of rigid body refinement in each case. In all cases, shifting one DARPin increased R_{free} by about 1.5%–3% and shifting both DARPins increased R_{free} by about 4.5%–5.5% (Table ST4). The appearance of positive and negative difference density clearly indicated that the new register was not correct (Fig. S14).

Figures were generated with PyMOL (DeLano Scientific LLC, Schrödinger).

Receptor internalization and degradation assay

To quantify internalization and degradation of MET upon DARPin treatment, we followed a protocol described elsewhere [50], which allows for homogenous processing of adherent cells. In brief, a HaloTag

MET receptor fusion was overexpressed in a stable Flp-In TREx HEK293 cell line. For the assay, cells were seeded 2 days before the first treatment, and then 1 day before treatment, expression was induced by addition of doxycycline to establish receptor expression for 24 h. DARPins (100 nM) were added at indicated time points (relative to the time of cell labeling).

In a first labeling step, a HaloTag ligand containing to Alexa Fluor 660 (HTL-AF660), which is completely cell-impermeable and therefore stains surface receptors only, was applied. In the second step, a cell-permeable HaloTag ligand containing tetramethyl rhodamine (HTL-TMR) was used to stain all receptor fusion remaining in intracellular compartments. Consequently, surface and internal receptor can be detected in separate channels, enabling us to obtain localization information and receptor quantitation. A commercially available dead-cell stain was further included to exclude permeabilized (dead) cells from analysis, for which all receptor would appear to be on the surface. Eventually, fluorescence intensities of single viable cells in the respective channels were recorded with a flow cytometer. Untreated cells were used for normalization, and relative surface and internal receptor levels were plotted for each treatment and time point.

Statistical analyses

Statistical analyses were performed using GraphPad Prism (La Jolla, CA, USA). All data are expressed as means ± standard deviation unless indicated otherwise.

Data availability

The coordinates and structure factors of the A3A/MET_{741}/$InlB_{321}$ complex have been deposited in the PDB with accession code 6GCU. Data supporting the findings of this study are available within the article and its Supplementary information Files or from the corresponding author upon reasonable request.

Acknowledgments

We would like to thank Dr. Birgit Dreier, Dr. Johannes Schilling and Dr. Martin Schwill for helpful discussions and for providing support and specific knowledge about DARPin engineering, binder selections and the expression and purification of the scFv 5D5. For help with binder screening and characterization, we want to thank Lars Wiedmer and Gianmarco Meier. Furthermore, the authors are grateful for the support and resources provided in the High Throughput Binder Selection facility (Department of Biochemistry, University of Zurich) by Dr. Jonas V. Schaefer and colleagues. We would like to thank Dr. Markus Schmid for valuable discussions and the help with flow cytometry measurements. Also, we would like to thank Dr. Morag Park (McGill University, Montreal, Canada) for providing cell lines. The synchrotron MX data were collected at beamline P13 operated by EMBL Hamburg at the PETRA III storage ring (DESY, Hamburg, Germany). We would like to thank Dr. Guillaume Pompidor for the assistance in using the beamline. Flow cytometry was performed with equipment maintained by the Flow Cytometry Facility of the University of Zurich. This work was supported by the Schweizerischer Nationalfonds (Switzerland) (Grant 310030B_166676 to A.P.). H.H.N. acknowledges funding by the German Science Foundation NI694/6-1. Work in E.G.'s laboratory was funded by Associazione Italiana contro Leucemie-Linfomi e Mieloma (AIL) Trentino.

Author Contributions: F.A. and A.P. designed the experiments. F.A., L.I., T.M., J.C.S. and F.K. performed the experiments. F.A., E.G., H.H.N. and A.P. wrote the manuscript; All authors edited the manuscript. E.G., H.H.N. and A.P. supervised the project.

Appendix A. Supplementary methods, figures and tables

Supplementary data to this article can be found online at https://doi.org/10.1016/j.jmb.2019.03.024.

Received 24 November 2018;
Received in revised form 19 March 2019;
Accepted 21 March 2019
Available online 28 March 2019

Keywords:
MET;
protein engineering;
X-ray crystallography;
DARPins;
biparatopic

Abbreviations used:
RTK, receptor tyrosine kinase; HGF/SF, hepatocyte growth factor/scatter factor; ECD, extracellular domain; TR-FRET, time-resolved fluorescence resonance energy transfer; SPR, surface plasmon resonance; IMAC, immobilized metal-ion affinity chromatography; PDB, Protein Data Bank.

References

[1] C.S. Cooper, M. Park, D.G. Blair, M.A. Tainsky, K. Huebner, C.M. Croce, et al., Molecular cloning of a new transforming gene from a chemically transformed human cell line, Nature 311 (1984) 29–33.

[2] D.P. Bottaro, J.S. Rubin, D.L. Faletto, A.M. Chan, T.E. Kmiecik, G.F. Vande Woude, et al., Identification of the hepatocyte growth factor receptor as the c-met proto-oncogene product, Science 251 (1991) 802–804.
[3] C. Birchmeier, W. Birchmeier, E. Gherardi, G.F. Vande Woude, Met, metastasis, motility and more, Nat. Rev. Mol. Cell Biol. 4 (2003) 915–925.
[4] C.G. Huh, V.M. Factor, A. Sanchez, K. Uchida, E.A. Conner, S.S. Thorgeirsson, Hepatocyte growth factor/c-met signaling pathway is required for efficient liver regeneration and repair, Proc. Natl. Acad. Sci. U. S. A. 101 (2004) 4477–4482.
[5] J. Chmielowiec, M. Borowiak, M. Morkel, T. Stradal, B. Munz, S. Werner, et al., C-met is essential for wound healing in the skin, J. Cell Biol. 177 (2007) 151–162.
[6] E. Gherardi, W. Birchmeier, C. Birchmeier, G. Vande Woude, Targeting MET in cancer: rationale and progress, Nat. Rev. Cancer 12 (2012) 89–103.
[7] L. Schmidt, F.M. Duh, F. Chen, T. Kishida, G. Glenn, P. Choyke, et al., Germline and somatic mutations in the tyrosine kinase domain of the MET proto-oncogene in papillary renal carcinomas, Nat. Genet. 16 (1997) 68–73.
[8] I.A. Lubensky, L. Schmidt, Z. Zhuang, G. Weirich, S. Pack, N. Zambrano, et al., Hereditary and sporadic papillary renal carcinomas with c-met mutations share a distinct morphological phenotype, Am. J. Pathol. 155 (1999) 517–526.
[9] W.S. Park, S.M. Dong, S.Y. Kim, E.Y. Na, M.S. Shin, J.H. Pi, et al., Somatic mutations in the kinase domain of the Met/hepatocyte growth factor receptor gene in childhood hepatocellular carcinomas, Cancer Res. 59 (1999) 307–310.
[10] J.H. Lee, S.U. Han, H. Cho, B. Jennings, B. Gerrard, M. Dean, et al., A novel germ line juxtamembrane Met mutation in human gastric cancer, Oncogene 19 (2000) 4947–4953.
[11] A. Lorenzato, M. Olivero, S. Patane, E. Rosso, A. Oliaro, P.M. Comoglio, et al., Novel somatic mutations of the MET oncogene in human carcinoma metastases activating cell motility and invasion, Cancer Res. 62 (2002) 7025–7030.
[12] S. Koochekpour, M. Jeffers, S. Rulong, G. Taylor, E. Klineberg, E.A. Hudson, et al., Met and hepatocyte growth factor/scatter factor expression in human gliomas, Cancer Res. 57 (1997) 5391–5398.
[13] S.L. Organ, M.S. Tsao, An overview of the c-MET signaling pathway, Ther. Adv. Med. Oncol. 3 (2011) S7–S19.
[14] J. Bean, C. Brennan, J.Y. Shih, G. Riely, A. Viale, L. Wang, et al., MET amplification occurs with or without T790M mutations in EGFR mutant lung tumors with acquired resistance to gefitinib or erlotinib, Proc. Natl. Acad. Sci. U. S. A. 104 (2007) 20932–20937.
[15] J.A. Engelman, K. Zejnullahu, T. Mitsudomi, Y. Song, C. Hyland, J.O. Park, et al., MET amplification leads to gefitinib resistance in lung cancer by activating ERBB3 signaling, Science 316 (2007) 1039–1043.
[16] B. Lutterbach, Q. Zeng, L.J. Davis, H. Hatch, G. Hang, N.E. Kohl, et al., Lung cancer cell lines harboring MET gene amplification are dependent on Met for growth and survival, Cancer Res. 67 (2007) 2081–2088.
[17] G.A. Smolen, R. Sordella, B. Muir, G. Mohapatra, A. Barmettler, H. Archibald, et al., Amplification of MET may identify a subset of cancers with extreme sensitivity to the selective tyrosine kinase inhibitor PHA-665752, Proc. Natl. Acad. Sci. U. S. A. 103 (2006) 2316–2321.
[18] E. Kankuri, D. Cholujova, M. Comajova, A. Vaheri, J. Bizik, Induction of hepatocyte growth factor/scatter factor by fibroblast clustering directly promotes tumor cell invasiveness, Cancer Res. 65 (2005) 9914–9922.
[19] L. Liu, W. Zeng, M. Chedid, Y. Zeng, S.-h. Tschang, Y. Tian, et al. Abstract 873: a novel MET-EGFR bispecific antibody LY3164530 shows advantage over combining MET and EGFR antibodies in tumor inhibition and overcome resistance. In: Proceedings of the 107th Annual Meeting of the American Association for Cancer Res.; 2016 Apr 16–20; New Orleans, LA. Philadelphia (PA): AACR; *Cancer Res.* **76** (14 Suppl) 2016, Abstract nr 873.
[20] H. Jin, R. Yang, Z. Zheng, M. Romero, J. Ross, H. Bou-Reslan, et al., MetMAb, the one-armed 5D5 anti-c-Met antibody, inhibits orthotopic pancreatic tumor growth and improves survival, Cancer Res. 68 (2008) 4360–4368.
[21] J.M. Lee, S.H. Lee, J.W. Hwang, S.J. Oh, B. Kim, S. Jung, et al., Novel strategy for a bispecific antibody: induction of dual target internalization and degradation, Oncogene 35 (2016) 4437–4446.
[22] T. Martens, N.O. Schmidt, C. Eckerich, R. Fillbrandt, M. Merchant, R. Schwall, et al., A novel one-armed anti-c-Met antibody inhibits glioblastoma growth in vivo, Clin. Cancer Res. 12 (2006) 6144–6152.
[23] S.L. Moores, M.L. Chiu, B.S. Bushey, K. Chevalier, L. Luistro, K. Dorn, et al., A novel bispecific antibody targeting EGFR and cMet is effective against EGFR inhibitor-resistant lung tumors, Cancer Res. 76 (2016) 3942–3953.
[24] F. Schelter, J. Kobuch, M.L. Moss, J.D. Becherer, P.M. Comoglio, C. Boccaccio, et al., A disintegrin and metalloproteinase-10 (ADAM-10) mediates DN30 antibody-induced shedding of the met surface receptor, J. Biol. Chem. 285 (2010) 26335–26340.
[25] T. Cloughesy, G. Finocchiaro, C. Belda-Iniesta, L. Recht, A.A. Brandes, E. Pineda, et al., Randomized, double-blind, placebo-controlled, multicenter phase II study of onartuzumab plus bevacizumab versus placebo plus bevacizumab in patients with recurrent glioblastoma: efficacy, safety, and hepatocyte growth factor and O(6)-methylguanine-DNA methyltransferase biomarker analyses, J. Clin. Oncol. 35 (2017) 343–351.
[26] J.C. Bendell, H. Hochster, L.L. Hart, I. Firdaus, J.R. Mace, J.J. McFarlane, et al., A phase II randomized trial (GO27827) of first-line FOLFOX plus bevacizumab with or without the MET inhibitor onartuzumab in patients with metastatic colorectal cancer, Oncologist 22 (2017) 264–271.
[27] V. Dieras, M. Campone, D.A. Yardley, G. Romieu, V. Valero, S.J. Isakoff, et al., Randomized, phase II, placebo-controlled trial of onartuzumab and/or bevacizumab in combination with weekly paclitaxel in patients with metastatic triple-negative breast cancer, Ann. Oncol. 26 (2015) 1904–1910.
[28] M.A. Shah, J.Y. Cho, I.B. Tan, N.C. Tebbutt, C.J. Yen, A. Kang, et al., A randomized phase II study of FOLFOX with or without the MET inhibitor onartuzumab in advanced adenocarcinoma of the stomach and gastroesophageal junction, Oncologist 21 (2016) 1085–1090.
[29] D.R. Spigel, T.J. Ervin, R.A. Ramlau, D.B. Daniel, J.H. Goldschmidt Jr., G.R. Blumenschein Jr., et al., Randomized phase II trial of onartuzumab in combination with erlotinib in patients with advanced non-small-cell lung cancer, J. Clin. Oncol. 31 (2013) 4105–4114.
[30] J. Qi, M.A. McTigue, A. Rogers, E. Lifshits, J.G. Christensen, P.A. Janne, et al., Multiple mutations and bypass mechanisms can contribute to development of acquired resistance to MET inhibitors, Cancer Res. 71 (2011) 1081–1091.
[31] M. Merchant, X. Ma, H.R. Maun, Z. Zheng, J. Peng, M. Romero, et al., Monovalent antibody design and mechanism of action of onartuzumab, a MET antagonist with anti-tumor activity as a therapeutic agent, Proc. Natl. Acad. Sci. U. S. A. 110 (2013) E2987–E2996.

[32] A. Plückthun, Designed ankyrin repeat proteins (DARPins): binding proteins for research, diagnostics, and therapy, Annu. Rev. Pharmacol. Toxicol. 55 (2015) 489–511.
[33] C. Jost, A. Plückthun, Engineered proteins with desired specificity: DARPins, other alternative scaffolds and bispecific IgGs, Curr. Opin. Struct. Biol. 27 (2014) 102–112.
[34] L. Rao, K. De Veirman, D. Giannico, I. Saltarella, V. Desantis, M. A. Frassanito, et al., Targeting angiogenesis in multiple myeloma by the VEGF and HGF blocking DARPin((R)) protein MP0250: a preclinical study, Oncotarget 9 (2018) 13366–13381.
[35] Y.L. Boersma, G. Chao, D. Steiner, K.D. Wittrup, A. Plückthun, Bispecific designed ankyrin repeat proteins (DARPins) targeting epidermal growth factor receptor inhibit A431 cell proliferation and receptor recycling, J. Biol. Chem. 286 (2011) 41273–41285.
[36] C. Jost, J. Schilling, R. Tamaskovic, M. Schwill, A. Honegger, A. Plückthun, Structural basis for eliciting a cytotoxic effect in HER2-overexpressing cancer cells via binding to the extracellular domain of HER2, Structure 21 (2013) 1979–1991.
[37] R. Tamaskovic, M. Schwill, G. Nagy-Davidescu, C. Jost, D.C. Schaefer, W.P. Verdurmen, et al., Intermolecular biparatopic trapping of ErbB2 prevents compensatory activation of PI3K/AKT via RAS-p110 crosstalk, Nat. Commun. 7 (2016), 11672.
[38] M.R. Mark, N.A. Lokker, T.F. Zioncheck, E.A. Luis, P.J. Godowski, Expression and characterization of hepatocyte growth factor receptor-IgG fusion proteins. Effects of mutations in the potential proteolytic cleavage site on processing and ligand binding, J. Biol. Chem. 267 (1992) 26166–26171.
[39] E. Gherardi, M.E. Youles, R.N. Miguel, T.L. Blundell, L. Iamele, J. Gough, et al., Functional map and domain structure of MET, the product of the c-met protooncogene and receptor for hepatocyte growth factor/scatter factor, Proc. Natl. Acad. Sci. U. S. A. 100 (2003) 12039–12044.
[40] H.K. Binz, M.T. Stumpp, P. Forrer, P. Amstutz, A. Plückthun, Designing repeat proteins: well-expressed, soluble and stable proteins from combinatorial libraries of consensus ankyrin repeat proteins, J. Mol. Biol. 332 (2003) 489–503.
[41] J. Schilling, J. Schoppe, A. Plückthun, From DARPins to LoopDARPins: novel LoopDARPin design allows the selection of low picomolar binders in a single round of ribosome display, J. Mol. Biol. 426 (2014) 691–721.
[42] A.Z. Lai, S. Cory, H. Zhao, M. Gigoux, A. Monast, M.C. Guiot, et al., Dynamic reprogramming of signaling upon Met inhibition reveals a mechanism of drug resistance in gastric cancer, Sci. Signal. 7 (2014) ra38.
[43] H.K. Binz, P. Amstutz, A. Kohl, M.T. Stumpp, C. Briand, P. Forrer, et al., High-affinity binders selected from designed ankyrin repeat protein libraries, Nat. Biotechnol. 22 (2004) 575–582.
[44] J. Stamos, R.A. Lazarus, X. Yao, D. Kirchhofer, C. Wiesmann, Crystal structure of the HGF beta-chain in complex with the Sema domain of the Met receptor, EMBO J. 23 (2004) 2325–2335.
[45] H.H. Niemann, V. Jäger, P.J. Butler, J. van den Heuvel, S. Schmidt, D. Ferraris, et al., Structure of the human receptor tyrosine kinase Met in complex with the *Listeria* invasion protein InlB, Cell 130 (2007) 235–246.
[46] C. Basilico, A. Hultberg, C. Blanchetot, N. de Jonge, E. Festjens, V. Hanssens, et al., Four individually druggable MET hotspots mediate HGF-driven tumor progression, J. Clin. Invest. 124 (2014) 3172–3186.
[47] M. Adachi, K.R. Katsumura, K. Fujii, S. Kobayashi, H. Aoki, M. Matsuzaki, Proteasome-dependent decrease in Akt by growth factors in vascular smooth muscle cells, FEBS Lett. 554 (2003) 77–80.
[48] O. Riesterer, D. Zingg, J. Hummerjohann, S. Bodis, M. Pruschy, Degradation of PKB/Akt protein by inhibition of the VEGF receptor/mTOR pathway in endothelial cells, Oncogene 23 (2004) 4624–4635.
[49] A. Bellacosa, T.O. Chan, N.N. Ahmed, K. Datta, S. Malstrom, D. Stokoe, et al., Akt activation by growth factors is a multiple-step process: the role of the PH domain, Oncogene 17 (1998) 313–325.
[50] J.C. Stüber, F. Kast, A. Plückthun, High-throughput quantification of surface protein internalization and degradation, ACS Chem. Biol. (2019) (in press).
[51] N.M. Frazier, T. Brand, J.D. Gordan, J. Grandis, N. Jura, Overexpression-mediated activation of MET in the Golgi promotes HER3/ERBB3 phosphorylation, Oncogene 38 (2019) 1936–1950.
[52] H.N. Mo, P. Liu, Targeting MET in cancer therapy, Chronic Dis. Transl. Med. 3 (2017) 148–153.
[53] K.H. Kim, H. Kim, Progress of antibody-based inhibitors of the HGF–cMET axis in cancer therapy, Exp. Mol. Med. 49 (2017) e307.
[54] J.G. Christensen, R. Schreck, J. Burrows, P. Kuruganti, E. Chan, P. Le, et al., A selective small molecule inhibitor of c-Met kinase inhibits c-Met-dependent phenotypes in vitro and exhibits cytoreductive antitumor activity in vivo, Cancer Res. 63 (2003) 7345–7355.
[55] P.K. Parikh, M.D. Ghate, Recent advances in the discovery of small molecule c-Met kinase inhibitors, Eur. J. Med. Chem. 143 (2018) 1103–1138.
[56] S. Arena, A. Pisacane, M. Mazzone, P.M. Comoglio, A. Bardelli, Genetic targeting of the kinase activity of the Met receptor in cancer cells, Proc. Natl. Acad. Sci. U. S. A. 104 (2007) 11412–11417.
[57] R. Babb, G. Chen, C. Daly, D. MacDonald, US Patent application US2018/0134794_A1.
[58] Y. Asaoka, M. Tada, T. Ikenoue, M. Seto, M. Imai, K. Miyabayashi, et al., Gastric cancer cell line Hs746T harbors a splice site mutation of c-Met causing juxtamembrane domain deletion, Biochem. Biophys. Res. Commun. 394 (2010) 1042–1046.
[59] B. Dreier, A. Plückthun, Ribosome display: a technology for selecting and evolving proteins from large libraries, Methods Mol. Biol. 687 (2011) 283–306.
[60] J. Hanes, A. Plückthun, In vitro selection and evolution of functional proteins by using ribosome display, Proc. Natl. Acad. Sci. U. S. A. 94 (1997) 4937–4942.
[61] C. Zahnd, E. Wyler, J.M. Schwenk, D. Steiner, M.C. Lawrence, N.M. McKern, et al., A designed ankyrin repeat protein evolved to picomolar affinity to Her2, J. Mol. Biol. 369 (2007) 1015–1028.
[62] R. Karlsson, P.S. Katsamba, H. Nordin, E. Pol, D.G. Myszka, Analyzing a kinetic titration series using affinity biosensors, Anal. Biochem. 349 (2006) 136–147.
[63] E. Gherardi, S. Sandin, M.V. Petoukhov, J. Finch, M.E. Youles, L.G. Ofverstedt, et al., Structural basis of hepatocyte growth factor/scatter factor and MET signalling, Proc. Natl. Acad. Sci. U. S. A. 103 (2006) 4046–4051.
[64] M. Cianci, G. Bourenkov, G. Pompidor, I. Karpics, J. Kallio, I. Bento, et al., P13, the EMBL macromolecular crystallography beamline at the low-emittance PETRA III ring for high- and low-energy phasing with variable beam focusing, J. Synchrotron Radiat. 24 (2017) 323–332.
[65] W. Kabsch, Integration, scaling, space-group assignment and post-refinement, Acta Crystallogr. D Biol. Crystallogr. 66 (2010) 133–144.

[66] P.R. Evans, G.N. Murshudov, How good are my data and what is the resolution? Acta Crystallogr. D Biol. Crystallogr. 69 (2013) 1204–1214.
[67] M.D. Winn, C.C. Ballard, K.D. Cowtan, E.J. Dodson, P. Emsley, P.R. Evans, et al., Overview of the CCP4 suite and current developments, Acta Crystallogr. D Biol. Crystallogr. 67 (2011) 235–242.
[68] A.J. McCoy, R.W. Grosse-Kunstleve, P.D. Adams, M.D. Winn, L.C. Storoni, R.J. Read, Phaser crystallographic software, J. Appl. Crystallogr. 40 (2007) 658–674.
[69] D.M. DiCara, D.Y. Chirgadze, A.R. Pope, A. Karatt-Vellatt, A. Winter, P. Slavny, et al., Characterization and structural determination of a new anti-MET function-blocking antibody with binding epitope distinct from the ligand binding domain, Sci. Rep. 7 (2017) 9000.
[70] P.V. Afonine, R.W. Grosse-Kunstleve, N. Echols, J.J. Headd, N.W. Moriarty, M. Mustyakimov, et al., Towards automated crystallographic structure refinement with phenix.refine, Acta Crystallogr. D Biol. Crystallogr. 68 (2012) 352–367.
[71] M.A. Kramer, S.K. Wetzel, A. Plückthun, P.R. Mittl, M.G. Grütter, Structural determinants for improved stability of designed ankyrin repeat proteins with a redesigned C-capping module, J. Mol. Biol. 404 (2010) 381–391.
[72] P. Emsley, B. Lohkamp, W.G. Scott, K. Cowtan, Features and development of Coot, Acta Crystallogr. D Biol. Crystallogr. 66 (2010) 486–501.